Chinese Journal of Natural Medicines

(±)-Talapyrones AF: six pairs of dimeric polyketide enantiomers with unusual 6/6/6 and 6/6/6/5 ring systems from *Talaromycesadpressus*

Meijia Zheng, Xinyi Zhao, Chenxi Zhou, Hong Liao, Qin Li, Yuling Lu, Bingbing Dai, Weiguang Sun, Ying Ye, Chunmei Chen, Yonghui Zhang, Hucheng Zhu

Citation: Meijia Zheng, Xinyi Zhao, Chenxi Zhou, Hong Liao, Qin Li, Yuling Lu, Bingbing Dai, Weiguang Sun, Ying Ye, Chunmei Chen, Yonghui Zhang, Hucheng Zhu, (±)-Talapyrones AF: six pairs of dimeric polyketide enantiomers with unusual 6/6/6 and 6/6/6/5 ring systems from *Talaromycesadpressus*, Chinese Journal of Natural Medicines, 2025, 23(8), 932-937. doi: 10.1016/S1875-5364(25)60928-9.

View online: https://doi.org/10.1016/S1875-5364(25)60928-9

Chinese Journal of Natural Medicines 23 (2025) 932-937

Contents lists available at ScienceDirect

Chinese Journal of Natural Medicines

journal homepage: www.cjnmcpu.com/

Original article

(±)-Talapyrones A–F: six pairs of dimeric polyketide enantiomers with unusual 6/6/6 and 6/6/6/5 ring systems from *Talaromyces adpressus*

Meijia Zheng[a], Xinyi Zhao[a], Chenxi Zhou[a,b], Hong Liao[a], Qin Li[a], Yuling Lu[a], Bingbing Dai[a], Weiguang Sun[a], Ying Ye[a], Chunmei Chen[a,*], Yonghui Zhang[a,*], Hucheng Zhu[a,*]

[a] *Hubei Key Laboratory of Natural Medicinal Chemistry and Resource Evaluation, School of Pharmacy, Tongji Medical College, Huazhong University of Science and Technology, Wuhan 430030, China*

[b] *School of Pharmacy, Shenyang Pharmaceutical University, Shenyang 110016, China*

ARTICLE INFO

Article history:
Received 27 August 2024
Revised 16 November 2024
Accepted 4 January 2025
Available online 20 August 2025

Keywords:
Polyketides
Talaromyces adpressus
Enantiomers
Structure elucidation
Biosynthetic pathways

ABSTRACT

(±)-Talapyrones A–F (**1**–**6**), six pairs of dimeric polyketide enantiomers featuring unusual 6/6/6 and 6/6/6/5 ring systems, were isolated from the fungus *Talaromyces adpressus*. Their structures were determined by spectroscopic analysis and HR-ESI-MS data, and their absolute configurations were elucidated using a modified Mosher's method and electronic circular dichroism (ECD) calculations. (±)-Talapyrones A–F (**1**–**6**) possess a 6/6/6 tricyclic skeleton, presumably formed through a Michael addition reaction between one molecule of *α*-pyrone derivative and one molecule of C_8 poly-*β*-keto chain. In addition, compounds **2**/**3** and **4**/**5** are two pairs of C-18 epimers, respectively. Putative biosynthetic pathways of **1**–**6** were discussed.

1. Introduction

Polyketides, mainly isolated from plants and microbes, are a large class of natural products exhibiting diverse structural characteristics and significant bioactivities. Among them, pyrone derivatives represent a notable category of polyketides [1, 2], which have been reported to exhibit various biological properties, such as cytotoxic, antioxidant, and antibacterial effects [1-4]. Their structural diversity and biological activities make them particularly valuable in pharmaceutical applications [5], as exemplified by inoscavin A, a pyrone compound isolated from the *Sanghuangporus vaninii*. Inoscavin A exerted its antitumor activity in an HT-29 colon cancer cell xenograft mouse model, indicating its potential as a therapeutic compound for colon cancer treatment [6]. Structurally, these fungal pyrone derivatives are mainly derived from polyketide pathways under the catalysis of polyketide synthases (PKSs), followed by structural modifications involving addition, enolization, and oxidation [7].

In recent years, polyketides have emerged as both a primary research focus and one of the predominant metabolite types in *Talaromyces* [8-12]. Species of *Talaromyces* are known to produce terpenoids [13-16], polyketides [17], steroids [18, 19], and diverse structural compounds [20-23], some of which show antibacterial, antiviral, NO inhibitory, and anti-inflammatory activities [13, 18, 24-27]. These findings have significantly motivated our investigation into structurally unique and bioactive metabolites from the genus of *Talaromyces*.

A chemical investigation of *T. adpressus* led to the isolation and identification of six pairs of dimeric polyketide enantiomers, (±)-talapyrones A–F (**1**–**6**), which represent the first examples of dimeric *α*-pyrone polyketides possess unexpected 6/6/6 and 6/6/6/5 ring systems (Fig. 1). This paper details the isolation, structural elucidation, plausible biogenetic pathway, and bioactivity evaluation of these compounds.

2. Results and discussion

(±)-Talapyrone A (**1**) was isolated as a colorless oil. High-resolution electrospray ionization mass spectrometry (HR-ESI-MS) established its molecular formula as $C_{18}H_{22}O_6$ based on $[M + Na]^+$ ion at *m/z* 357.1327 (Calcd. for $C_{18}H_{22}O_6Na$, 357.1314), corresponding to eight degrees of unsaturation. The infrared (IR) spectrum of **1** revealed the presence of hydroxyl (3429 cm^{-1}) and carbonyl (1699 cm^{-1}) groups. The 1D nuclear magnetic resonance (NMR) (Table 1) and heteronuclear single quantum coherence (HSQC) spectra of **1** revealed 18 carbon resonances, including two methyls [δ_H 1.73, δ_C 9.4; δ_H 1.00, δ_C 14.2], one methoxy group (δ_H 3.91, δ_C 57.3), and five methylenes, one of which was oxygenated (δ_H 3.86/3.41, δ_C 58.8). Two methine carbons were identified, including one olefinic (δ_H 5.60, δ_C 88.6). Eight nonprotonated carbons were observed, including one conjugated ketone

* Corresponding author.
E-mail addresses: chenchuanmei@hust.edu.cn (C. Chen); zhangyh@mails.tjmu.edu.cn (Y. Zhang); zhuhucheng@hust.edu.cn (H. Zhu)

https://doi.org/10.1016/S1875-5364(25)60928-9

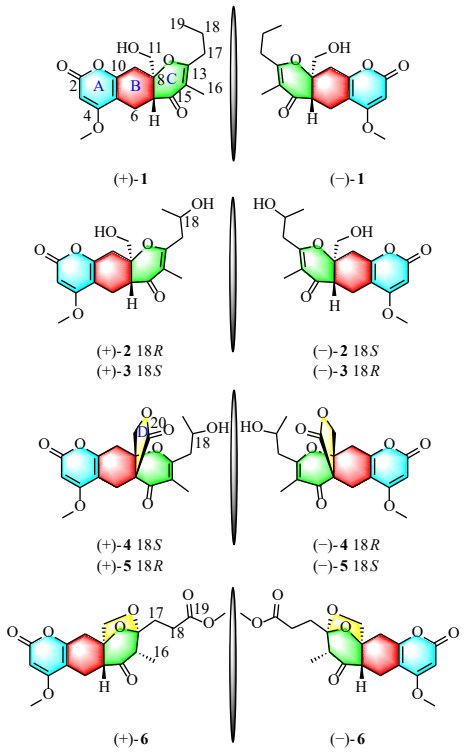

Fig. 1 Structures of **1**–**6**.

carbonyl (δ_C 194.1), one conjugated ester carbonyl (δ_C 166.9), and six olefinic/aromatic carbons (δ_C 88.6, 109.0, 110.1, 157.2, 171.4, and 172.2). Of the eight degrees of unsaturation, five are accounted for by three double bonds and two carbonyl groups. The remaining three degrees necessitate a tricyclic framework to fully satisfy the molecular unsaturation, thereby supporting the presence of a compact polycyclic core structure in compound **1**.

The UV absorption at 282 nm and IR absorptions at 1699 and 1568 cm^{-1} indicated the presence of an α-pyrone moiety [28-30]. Heteronuclear multiple bond correlations (HMBCs) (Fig. 2) from H-3 to C-2, C-4, and C-5, and from H_2-6 to C-4, C-5, and C-10, along with these characteristic chemical shifts, established the structure of an α-pyrone (ring A) in **1**. In addition, HMBCs from H-7 to C-8 and C-15, from Me-16 to C-13, C-14, and C-15, H_2-17 to C-13 and C-14, together with the ^1H–^1H COSY cross-peaks (Fig. 2) of H_2-17/H_2-18/Me-19, confirmed the presence of a γ-pyrone (ring C). Furthermore, the ^1H–^1H correlation spectroscopy (COSY) cross-peaks of H_2-6/H-7, as well as HMBCs from H_2-6 and H_2-9 to C-5, C-7, C-8, and C-10, H_2-11 to C-7, C-8, and C-9, revealed the connection between rings A and C *via* C-6 and C-9, enabling the assenbly of ring B. Thus, the planar structure of **1** with a novel tricyclic 6/6/6 carbon skeleton was elucidated.

The relative configuration of **1** was deduced by analysis of its nuclear Overhauser effect spectroscopy (NOESY) spectrum. NOESY correlations (Fig. 3) of H_2-11/H-6b, H-7/H-6a, and H-7/H-9b indicated the *trans* relationship of CH_2-11 and H-7. The optical rotation data (close to zero) along with the undetectable Cotton effect in the ECD spectrum, suggested the racemic feature of **1**. Subsequently, chiral resolution of **1** was successfully performed to obtain (+)-**1** and (−)-**1**, in a ratio of approximately 1∶1, on a chiral column eluting with MeCN–H_2O (37∶63, *V*/*V*) (Fig. S1). The absolute configurations of (+)-**1** and (−)-**1** were established as 7*R*,8*R* and 7*S*,8*S*, respectively, through comparison of their experimental ECD spectra with calculated curves (Fig. 4).

(±)-Talapyrone B (**2**) was isolated as a white powder. Its molecular formula, $C_{18}H_{22}O_7$, was established by HR-ESI-MS based on an $[M + Na]^+$ ion at *m*/*z* 373.1263 (Calcd. for $C_{18}H_{22}O_7Na$, 373.1263), indicating eight degrees of unsaturation. A comparison of the ^1H and ^{13}C NMR data (Table 1) of **2** with those of **1** revealed a high degree of structural similarity, except for the replacement of a methylene group with an oxygenated methine (δ_C 65.0). This substitution, together with the additional oxygen atom in the molecular formula, supported the presence of an extra hydroxyl group in **2**. The ^1H–^1H COSY cross-peaks of H_2-17/H-18/Me-19 and the HMBCs from H_2-17 to C-13, C-14, C-18, and C-19 established the position of the hydroxyl group at C-18.

(±)-Talapyrone C (**3**) displayed the same molecular formula of $C_{18}H_{22}O_7$ as that of **2**, as shown by its HR-ESI-MS data with an $[M + Na]^+$ ion at *m*/*z* 373.1263 (Calcd. for $C_{18}H_{22}O_7Na$, 373.1263). The ^1H and ^{13}C NMR data (Table 1) of **3** closely resembled those of **2**, with the only difference being minor downfield shifts at C-17 ($\Delta\delta_C$ +0.6), C-18 ($\Delta\delta_C$ +0.6), and C-19 ($\Delta\delta_C$ +0.5), suggesting epimerization at the C-18 stereocenter.

The relative configurations of compounds **2** and **3** were determined by NOESY experiments, which exhibited key correlations consistent with those observed in **1** (Fig. 3), including H_2-11/H-6b, H-7/H-6a, and H-7/H-9b. To resolve their absolute configurations, racemic **2** and **3** were subjected to chiral HPLC, yield-

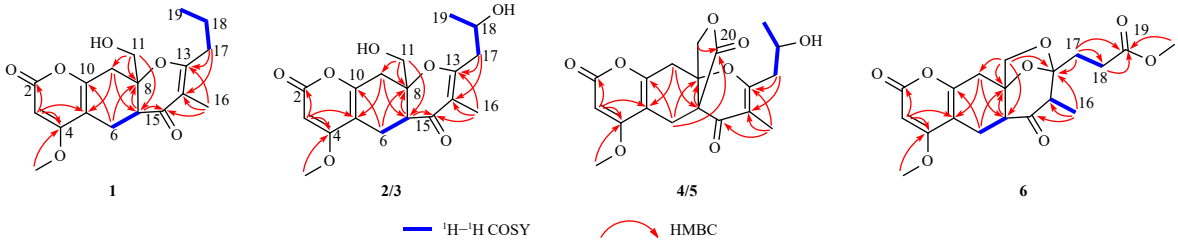

Fig. 2 Key ^1H–^1H COSY and HMBC correlations of compounds **1**–**6**.

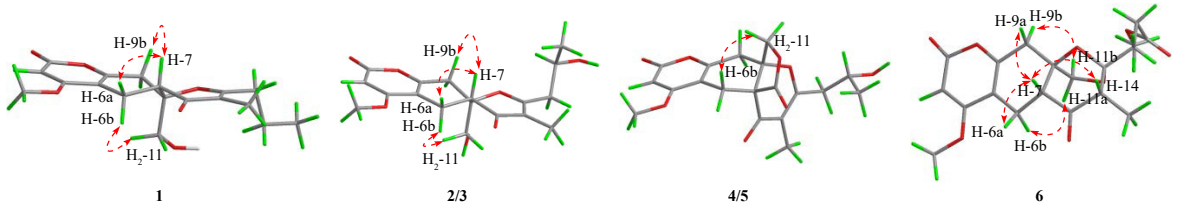

Fig. 3 Key NOESY correlations of compounds **1**–**6**.

ing (+)-**2**, (−)-**2**, (+)-**3**, and (−)-**3** (Figs. S2 and S3). Subsequently, a modified Mosher's method was conducted to determine the absolute configuration of C-18 of (−)-**3**, and the significant $\Delta\delta_H$ values ($\Delta\delta_H = \delta_{S\text{-MTPA-ester}} - \delta_{R\text{-MTPA-ester}}$) observed for protons adjacent to C-18 (Fig. 5) supported an *R*-configuration at this center, based on modified Mosher's method criteria [31]. Therefore, their absolute configurations were finally elucidated as 7*R*,8*R*,18*R* for (+)-**2**, 7*S*,8*S*,18*S* for (−)-**2**, 7*R*,8*R*,18*S* for (+)-**3**, and 7*S*,8*S*,18*R* for (−)-**3** by comparing the experimental and calculated ECD spectra (Fig. 4), respectively.

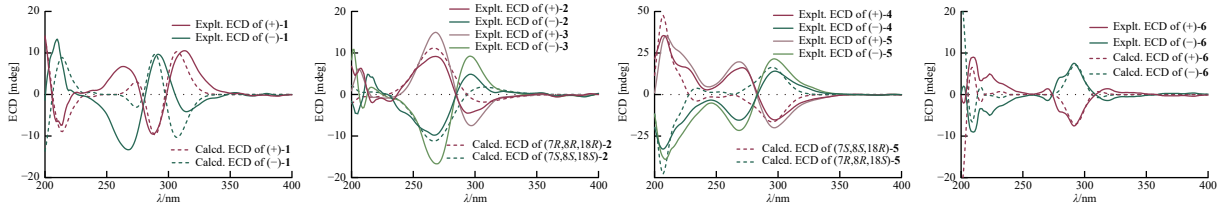

Fig. 4 Experimental and calculated ECD spectra of compounds **1**–**6**.

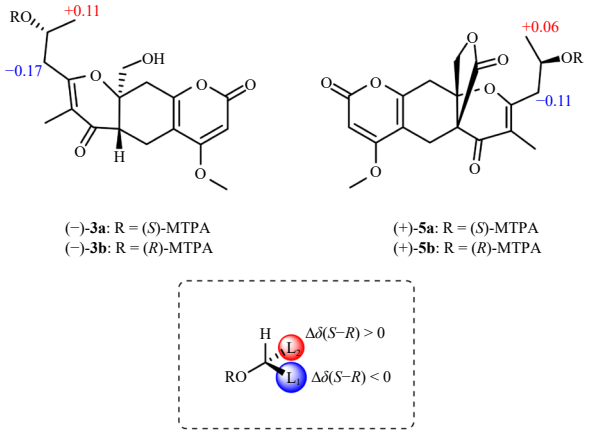

(−)-**3a**: R = (*S*)-MTPA
(−)-**3b**: R = (*R*)-MTPA
(+)-**5a**: R = (*S*)-MTPA
(+)-**5b**: R = (*R*)-MTPA

Fig. 5 $\Delta\delta_{H\ (S-R)}$ values for the (*R*)- and (*S*)-MTPA esters of compounds (−)-**3** and (+)-**5**.

(±)-Talapyrone D (**4**) was obtained as a colorless oil. Its molecular formula, $C_{19}H_{20}O_8$, was deduced from its HR-ESI-MS data with an $[M + Na]^+$ ion at *m/z* 399.1063 (Calcd. for $C_{19}H_{20}O_8Na$, 399.1056), corresponding to 10 degrees of unsaturation. A comparison of the ^1H and ^{13}C NMR data (Table 1) of **4** and **2** revealed that **4** differed from **2** in the replacement of the methine group (CH-7) in **2** by a quaternary carbon (δ_C 53.5) and the presence of an additional ester carbonyl C-20 (δ_C 173.3) at C-7, as confirmed by the HMBC correlations (Fig. 2) from H_2-6 to C-7 and C-20. The key HMBC from H_2-11 to C-20 suggested the presence of a five-membered lactone unit (ring D).

(±)-Talapyrone E (**5**) displayed the same molecular formula of $C_{19}H_{20}O_8$ as **4**, as evidenced by its HR-ESI-MS data with an $[M + Na]^+$ ion at *m/z* 399.1053 (Calcd. for $C_{19}H_{20}O_8Na$, 399.1056). Analysis of the ^1H NMR data (Table 1) revealed that the only differences between compounds **4** and **5** were the chemical shifts of C-17 ($\Delta\delta_C$ +0.4) and C-18 ($\Delta\delta_C$ +0.3), suggesting that **4** and **5** were a pair of C-18 epimers.

The bonds of C-7/C-20 and C-8/C-11 of **4** and **5** were cofacial due to the presence of the ring D; however, the relative configuration of C-18 could not be determined by the NOESY spectrum. Based on their optical rotation values (close to zero) and the absence of Cotton effects in their ECD spectra, **4** and **5** were determined to be racemates. Subsequently, **4** and **5** were successfully separated by chiral high-performance liquid chromatography (HPLC) (Figs. S4 and S5). Finally, the absolute configuration of C-18 of (+)-**5** was defined as *R* by a modified Mosher's method (Fig. 5). A comparison between the calculated and experimental ECD curves (Fig. 4) enabled the final elucidation of their absolute configurations as 7*S*,8*S*,18*S* for (+)-**4**, 7*R*,8*R*,18*R* for (−)-**4**, 7*S*,8*S*,18*R* for (+)-**5**, and 7*R*,8*R*,18*S* for (−)-**5**, respectively.

(±)-Talapyrone F (**6**) was afforded as a colorless oil. Its molecular formula was determined to be $C_{19}H_{22}O_8$ on the basis of the HR-ESI-MS data with an $[M + Na]^+$ ion at *m/z* 401.1229 (Calcd. for $C_{19}H_{22}O_8Na$, 401.1212), corresponding to nine degrees of unsaturation. A comparison of the NMR data (Table 1) of **6** with those of **1** implied that they possessed a similar structure. However, the double bond $\Delta^{13,14}$ in ring C was reduced, which was confirmed by the ^1H–^1H COSY cross-peaks (Fig. 2) of H-14/H_3-16 and the HMBCs (Fig. 2) from H_2-17 to C-13 and C-14. Furthermore, the HMBCs from H_2-11 to C-13 combined with the chemical shift of C-13 (δ_C 110.0) suggested the presence of a hemiketal group. In addition, the HMBCs from H_2-17, H_2-18, and 19-OMe to C-19 established the side chain. Thus, the planar structure of **6** was elucidated, featuring a novel tetracyclic 6/6/6/5-fused architecture. The NOESY interactions (Fig. 3) between H-7/H-14, H-7/H-6a, and H-7/H-9a indicated that these protons were cofacial and assigned to the *β*-orientation, while the cross-peaks between H-6b/H-11a and H-9b/H-11b indicated the *α*-orientation of the ether ring between C-11 and C-13. Chiral HPLC separation of **6** yielded optically pure compounds (+)-**6** and (−)-**6** (Fig. S6), with absolute configurations determined by ECD calculations (Fig. 4) as 7*R*,8*R*,13*S*,14*R* and 7*S*,8*S*,13*R*,14*S*, respectively.

Compounds **1**–**6** were a series of novel dimeric polyketide enantiomers featuring 6/6/6 and 6/6/6/5 ring systems. Their rational biosynthetic pathways are illustrated in Scheme 1. The proposed precursors $\mathbf{i_a}$ and $\mathbf{i_b}$ are formed *via* the polyketide pathway originating from acetyl-CoA and malonyl-CoA through Claisen reaction, cyclization, methylation, and hydroxylation. Subsequently, intermediates $\mathbf{i_a}$ and $\mathbf{i_b}$ experienced Michael addition and vital aldol reactions to generate the key intermediate **ii**. A hemiacetal **iii** formed when C-8-OH attacks the carbonyl in **ii**. The $\Delta^{13,14}$ double bond developed through dehydration to afford **iv**. After decarboxylation, compounds **2** and **3** were produced, which then underwent reduction at C-18 to produce **1**. Compounds **4** and **5** are derived from **iv** through intramolecular esterification. Alternatively, intermediate **iii** underwent sequential intramolecular etherification, oxidation, decarboxylation, and esterification to yield compound **6**.

In the bioactivity assays, compounds **1**–**6** were evaluated for *in vitro* cytotoxicity and immunosuppressive activity according to previously reported methods [32,33]; however, none exhibited significant activities. In addition, all isolates were tested for the anti-lipid-accumulation activities using free fatty acid (FFA)-induced HepG2 cells by Oil Red O (ORO) staining assay (Fig. S7).

3. Experimental

3.1. General experimental procedures

Optical rotations were measured on a PerkinElmer 341 polarimeter (Rudolph Research Analytical, Hackettstown, NJ, USA)

Table 1 ^{1}H NMR (400 MHz) and ^{13}C (100 MHz) data for compounds **1**–**6** (*J* in Hz).

No.	**1**[a]		**2**[b]		**3**[b]		**4**[a]		**5**[a]		**6**[b]	
	δ_H	δ_C	δ_H	δ_C	δ_H	δ_C	δ_H	δ_C	δ_H	δ_C	δ_H	δ_C
2		166.9		162.9		163.0		165.9		165.9		162.7
3	5.60 s	88.6	5.59 s	87.6	5.60 s	87.6	5.59 s	89.0	5.59 s	89.0	5.60 s	87.7
4		172.2		169.5		169.6		171.1		171.2		169.5
5		109.0		106.5		106.5		106.7		106.7		106.1
6a	2.98 m	19.5	2.74 dd (17.5, 6.3)	18.2	2.74 dd (17.5, 6.3)	18.2	3.67 d (17.8)	23.7	3.67 d (17.4)	23.7	2.69 dd (17.7, 6.0)	18.6
6b	2.22 m		2.07 dd (17.5, 11.6)		2.07 dd (17.5, 11.6)		2.60 d (17.8)		2.55 d (17.4)		2.27 dd (17.7, 11.1)	
7	3.17 m	45.7	3.16 m	43.8	3.17 m	43.9		53.5		53.6	2.97 dd (11.1, 6.0)	49.4
8		82.4		81.1		81.2		86.0		86.3		80.3
9a	3.21 m	36.4	3.06 d (17.3)	34.8	3.07 d (17.2)	34.8	3.14 dd (6.8, 2.0)	31.2	3.17 m	30.6	3.31 m	34.2
9b	2.94 m		2.87 d (17.3)		2.87 d (17.2)						2.78 d (17.4)	
10		157.2		155.5		155.5		155.4		155.5		154.5
11a	3.86 d (12.4)	58.8	3.70 m	56.4	3.74 dd (13.9, 4.2)	56.6	4.65 d (10.3)	74.4	4.64 d (10.4)	74.7	3.82 d (8.0)	71.5
11b	3.41 d (12.4)		3.19 m		3.22 m		4.48 d (10.3)		4.50 d (10.4)		3.43 d (8.0)	
13		171.4		166.4		166.1		169.9		169.8		110.0
14		110.1		109.3		110.0		111.4		111.9	2.82 dd (6.9 1.4)	52.5
15		194.1		191.3		191.3		184.7		184.6		205.5
16	1.73 s	9.4	1.65 s	9.2	1.66 s	9.4	1.78 s	10.0	1.78 s	10.0	0.97 d (6.8)	8.5
17a	2.37 m	35.2	2.46 dd (13.3, 5.7)	41.7	2.55 dd (14.0, 7.5)	41.1	2.54 m	43.0	2.65 dd (14.0, 8.7)	42.6	2.42 m	27.3
17b			2.30 dd (13.3, 7.6)		2.32 dd (14.0, 5.2)				2.41 dd (14.0, 4.5)			
18	1.68 q (7.5)	21.1	3.95 m	65.0	4.03 q (6.3)	64.4	4.09 dd (6.2, 1.3)	66.6	4.12 m	66.3	2.07 m	29.1
19	1.00 t (7.4)	14.2	1.14 d (6.2)	23.6	1.13 d (6.2)	23.1	1.24 d (6.2)	24.0	1.24 d (6.2)	23.9		173.1
20								173.3		173.4		
4-OCH_3	3.91 s	57.3	3.84 s	56.7	3.84 s	56.7	3.91 s	57.5	3.91 s	57.5	3.84 s	56.7

[a] Recorded in CD_3OD; [b] Recorded in DMSO-d_6.

with sodium light (λ_{max} = 589 nm). UV spectra were recorded on a SolidSpec-3700 spectrophotometer (Shimadzu, Kyoto, Japan) using CH_3OH. ECD spectra were determined on a Jasco 810 spectrometer (JASCO, Tokyo, Japan). IR spectra were collected from a Nicolet iS50R FT-IR spectrophotometer (Thermo Scientific, Waltham, US) with KBr pellets. 1D (^{1}H, ^{13}C, and DEPT) and 2D (HSQC, HMBC, ^{1}H–^{1}H COSY and NOESY) NMR spectra were recorded using a Bruker AM-400 NMR spectrometer (Bruker, Karlsruhe, Germany) with CD_3OD and DMSO as solvents. HR-ESI-MS data were obtained using a Bruker microOTOF II spectrometer (Bruker, Karlsruhe, Germany). Silica gel (200–300 mesh; Qingdao Marine Chemical, Inc., China), Sephadex LH-20 (Merck, Darmstadt, Germany), and Lichroprep RP-C_{18} gel (40–63 μm, Merck, Darmstadt, Germany), were applied for column chromatography (CC). An Agilent 1220 with a UV detector using an RP-C_{18} column (5 μm, 10 mm × 250 mm, Welch Ultimate XB-C_{18}) was applied for semi-preparative HPLC. Silica gel 60 F_{254} and RP-C_{18} F_{254} plates were applied for TLC detection, and spots were visualized by spraying heated silica gel plates with 10% H_2SO_4 in EtOH.

3.2. Fungal material

The fungal strain *Talaromyces adpressus* was isolated from sediment samples collected in Hainan Province, China. Taxonomic identification was confirmed through a combination of morphological characterization and internal transcribed spacer (ITS) region sequencing of ribosomal DNA (GenBank No. MZ373307). The authenticated strain has been deposited in the culture collection of the School of Pharmacy, Tongji Medical College, Huazhong University of Science and Technology.

3.3. Extraction and isolation

The strain *T. adpressus* was cultivated on potato dextrose agar (PDA) plates at 28 °C for 4 d. The resulting mycelial mats were cut into small cubes (0.3 cm × 0.3 cm × 0.3 cm) and inoculated into 300 sterilized Erlenmeyer flasks (1 L), each containing 200 g of rice and 200 mL of distilled water. The flasks were incubated for 30 d at 28 °C. The rice cultures were extracted with EtOAc at room temperature (10 ×). The combined organic phases were concentrated under reduced pressure to yield 500 g of crude extract. This extract was subjected to silica gel CC, eluted with a petroleum ether/EtOAc gradient (10∶1 to 1∶1, *V/V*), affording four major fractions (A–D). Fraction D (80 g) was further purified using ODS CC with a MeOH/H_2O gradient (20∶80–100∶0), yielding nine subfractions (D1–D9). Fraction D2 (4.2 g)

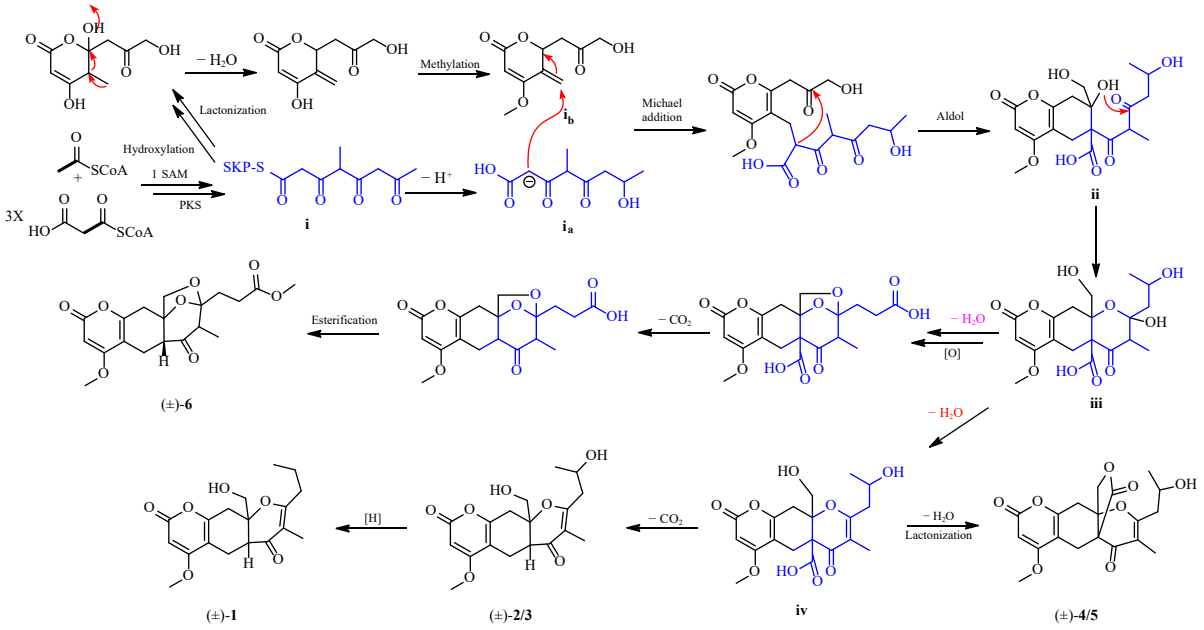

Scheme 1 Hypothetical biosynthetic pathways of **1**–**6**.

was further refined by Sephadex LH-20 CC and isostatically eluted with MeOH, affording fractions D2.1–D2.3. Subsequent separation of D2.2 (1.6 g) using a CH_2Cl_2/MeOH gradient (70∶1–20∶1) produced six fractions D2.2.1–D2.2.6. Additionally, fraction D2.2.4 (96.0 mg) was further separated *via* semipreparative HPLC with MeCN/H_2O (22∶78, *V*/*V*, 2.0 mL·min^{-1}) to produce compound **4** (3.2 mg, t_R 50 min) and **5** (5.8 mg, t_R 60 min). Compound **4** was separated by chiralpak IA column eluted with hexane/2-propanol (86∶14, *V*/*V*, 2.0 mL·min^{-1}) to give (+)-**4** (1.3 mg, t_R 32.5 min) and (−)-**4** (1.5 mg, t_R 28.5 min). Compound **5** was separated by chiralpak IA column eluted with hexane/2-propanol (81∶19, *V*/*V*, 2.0 mL·min^{-1}) to give (+)-**5** (3.1 mg, t_R 31.0 min) and (−)-**5** (2.5 mg, t_R 13.0 min). Fraction D2.2.5 (170.0 mg) was further separated *via* semipreparative HPLC with MeOH/H_2O (40∶60, *V*/*V*, 2.0 mL·min^{-1}) to produce compound **2** (5.5 mg, t_R 28 min). Compound **2** was separated by chiralpak IA column eluted with MeCN/H_2O (18.5∶81.5, *V*/*V*, 1.0 mL·min^{-1}) to give (+)-**2** (2.5 mg, t_R 9.0 min) and (−)-**2** (2.8 mg, t_R 12.0 min). Fraction D3 (2.0 g) was further refined by Sephadex LH-20 CC and isostatically eluted with MeOH to obtain fractions D3.1–D3.3. Then, fraction D3.1 (950.0 mg) was further separated with CH_2Cl_2/MeOH (70∶1–20∶1) to give fractions D3.1.1–D3.1.8. Fraction D3.1.5 (68.0 mg) was further separated *via* semipreparative HPLC with MeCN/H_2O (23∶77, *V*/*V*, 2.0 mL·min^{-1}) to produce compound **3** (10.9 mg, t_R 25 min). Compound **3** was separated by chiralpak IA column eluted with MeCN/H_2O (20∶80, *V*/*V*, 1.0 mL·min^{-1}) to give (+)-**3** (3.0 mg, t_R 22.5 min) and (−)-**3** (3.8 mg, t_R 40.0 min). Additionally, fraction D3.2 (350.0 mg) was further separated with CH_2Cl_2/MeOH (70∶1–20∶1) to give fractions D3.2.1–D3.2.4. Fraction D3.2.4 (68.0 mg) was further separated *via* semipreparative HPLC with MeOH/H_2O (53∶47, *V*/*V*, 2.0 mL·min^{-1}) to produce compound **6** (4.6 mg, t_R 28 min). Compound **6** was separated by chiralpak IA column eluted with MeCN/H_2O (40∶60, *V*/*V*, 1.0 mL·min^{-1}) to give (+)-**6** (2.4 mg, t_R 14.0 min) and (−)-**6** (1.8 mg, t_R 17.5 min). Fraction D4 (1.3 g) was fractionated by silica gel-column chromatography (CC) eluted with CH_2Cl_2/MeOH system (500∶1–30∶1) to give fractions D4.1–D4.16 by the TLC analysis. Then, fraction D4.7 (61.2 mg) was further repeated semipreparative HPLC with MeOH/H_2O (55∶45, *V*/*V*, 2.0 mL·min^{-1}) to obtain compound **1** (5.2 mg, t_R 38 min). Compound **1** was separated by chiralpak IA column eluted with MeCN/H_2O (37∶63, *V*/*V*, 1.0 mL·min^{-1}) to give (+)-**1** (1.1 mg, t_R 12.5 min) and (−)-**1** (0.8 mg, t_R 25.0 min).

Talapyrone A (**1**): UV (MeOH) λ_{max} (log ε) 205 (4.26), 282 (3.97) nm; IR (KBr) ν_{max} 3429, 1699, 1610, 1568, 1237, 1205, 812 cm^{-1}; ^{1}H and ^{13}C NMR data (Table 1); HR-ESI-MS *m*/*z* 357.1327 [M + Na]$^+$ (Calcd. for $C_{18}H_{22}O_6Na$, 357.1314).

(+)-**1**: colorless oil; $[\alpha]_D^{25}$ +83 (*c* 0.1, MeOH); ECD (MeOH) λ_{max} ($\Delta\varepsilon$) 211 (−4.56), 265 (+2.77), 287 (−3.94), 314 (+4.30) nm.

(−)-**1**: colorless oil; $[\alpha]_D^{25}$ −82 (*c* 0.1, MeOH); ECD (MeOH) λ_{max} ($\Delta\varepsilon$) 211 (+6.49), 268 (−5.43), 292 (+4.02), 315 (−1.70) nm.

Talapyrone B (**2**): UV (MeOH) λ_{max} (log ε) 201 (4.51), 281 (4.18) nm; IR (KBr) ν_{max} 3331, 1694, 1612, 1567, 1263, 811 cm^{-1}; ^{1}H and ^{13}C NMR data (Table 1); HR-ESI-MS *m*/*z* 373.1263 [M + Na]$^+$ (Calcd. for $C_{18}H_{22}O_7Na$, 373.1263).

(+)-**2**: white powder; $[\alpha]_D^{25}$ +16 (*c* 0.1, MeOH); ECD (MeOH) λ_{max} ($\Delta\varepsilon$) 267 (+3.91), 295 (−1.92) nm.

(−)-**2**: white powder; $[\alpha]_D^{25}$ −13 (*c* 0.1, MeOH); ECD (MeOH) λ_{max} ($\Delta\varepsilon$) 267 (−2.13), 295 (+1.03) nm.

Talapyrone C (**3**): UV (MeOH) λ_{max} (log ε) 203 (4.43), 285 (4.14) nm; IR (KBr) ν_{max} 3360, 1704, 1612, 1568, 1259, 815 cm^{-1}; ^{1}H and ^{13}C NMR data (Table 1); HR-ESI-MS *m*/*z* 373.1263 [M + Na]$^+$ (Calcd. for $C_{18}H_{22}O_7Na$, 373.1263).

(+)-**3**: white powder; $[\alpha]_D^{25}$ +89 (*c* 0.1, MeOH); ECD (MeOH) λ_{max} ($\Delta\varepsilon$) 268 (+12.76), 296 (−6.48) nm.

(−)-**3**: white powder; $[\alpha]_D^{25}$ −45 (*c* 0.1, MeOH); ECD (MeOH) λ_{max} ($\Delta\varepsilon$) 269 (−7.08), 297 (+3.93) nm.

Talapyrone D (**4**): UV (MeOH) λ_{max} (log ε) 204 (4.22), 282 (3.98) nm; IR (KBr) ν_{max} 3458, 1788, 1697, 1573, 1255, 1206, 804 cm^{-1}; ^{1}H and ^{13}C NMR data (Table 1); HR-ESI-MS *m*/*z* 399.1063 [M + Na]$^+$ (Calcd. for $C_{19}H_{20}O_8Na$, 399.1056).

(+)-**4**: colorless oil; $[\alpha]_D^{25}$ +87 (*c* 0.1, MeOH); ECD (MeOH) λ_{max} ($\Delta\varepsilon$) 206 (+17.15), 272 (+7.04), 297 (−6.94) nm.

(−)-**4**: colorless oil; $[\alpha]_D^{25}$ −101 (*c* 0.1, MeOH); ECD (MeOH) λ_{max} ($\Delta\varepsilon$) 207 (−14.88), 269 (−7.03), 298 (+6.43) nm.

Talapyrone E (**5**): UV (MeOH) λ_{max} (log ε) 205 (4.23), 282 (3.98) nm; IR (KBr) ν_{max} 3432, 1788, 1698, 1572, 1255, 1205, 804 cm^{-1}; ^{1}H and ^{13}C NMR data (Table 1); HR-ESI-MS *m*/*z* 399.1053 [M + Na]$^+$ (Calcd. for $C_{19}H_{20}O_8Na$, 399.1056).

(+)-**5**: colorless oil; $[\alpha]_D^{25}$ +106 (*c* 0.1, MeOH); ECD (MeOH) λ_{max} ($\Delta\varepsilon$) 208 (+17.03), 268 (+9.01), 297 (−9.13) nm.

(−)-**5**: colorless oil; $[\alpha]_D^{25}$ −108 (*c* 0.1, MeOH); ECD (MeOH) λ_{max} ($\Delta\varepsilon$) 207 (−20.38), 269 (−9.92), 296 (+9.85) nm.

Talapyrone F (**6**): UV (MeOH) λ_{max} (log ε) 203 (4.35), 283 (3.84) nm; IR (KBr) ν_{max} 3424, 1720, 1570, 1248, 1203, 814 cm^{-1}; ^1H and ^{13}C NMR data (Table 1); HR-ES-IMS *m/z* 401.1229 [M + Na]$^+$ (Calcd. for $C_{19}H_{22}O_8Na$, 401.1212).

(+)-**6**: colorless oil; $[\alpha]_D^{25}$ +43 (*c* 0.1, MeOH); ECD (MeOH) λ_{max} ($\Delta\varepsilon$) 208 (+1.80), 292 (−0.91), 318 (+0.81) nm.

(−)-**6**: colorless oil; $[\alpha]_D^{25}$ −60 (*c* 0.1, MeOH); ECD (MeOH) λ_{max} ($\Delta\varepsilon$) 208 (−1.80), 292 (+0.91), 318 (−0.81) nm.

3.4. ECD calculation

The detailed procedures and methods for the ECD calculation of **1**–**6** were provided in the Supporting information.

3.5. Anti-lipid-accumulation activity

HepG2 cells were seeded into six-well plates at a density of 1 × 10^6 cells per well and allowed to adhere under standard culture conditions. Following adherence, each test compound was added at a defined concentration and incubated for 24 h. Subsequently, the cells were exposed to 0.2 mmol·L^{-1} FFA for an additional 24 h, after which the culture medium was aspirated, and the cells were washed twice with phosphate-buffered saline (PBS). A staining wash solution was then applied to each well to cover the cells and incubated for 20 s before removal. ORO staining working solution was added, and the cells were stained for 10–20 min at room temperature. Finally, intracellular lipid droplets were visualized under a Nikon Eclipse Ci microscope.

Funding

This work was supported by the National Key Research and Development Program of China (No. 2021YFA0910500), the National Natural Science Foundation of China (Nos. U22A20380, 82173706, and 82104028), and the Science and Technology Major Project of Hubei Province (No. 2021ACA012).

Supporting information

Supporting information for this work can be obtained by contacting the corresponding authors *via* E-mail.

Declaration of competing interest

These authors have no conflict of interest to declare.

References

1 Zhao SS, Tian KL, Li Y, et al. Enantiomeric dibenzo-*α*-pyrone derivatives from *Alternaria alternata* ZHJG5 and their potential as agrochemicals. *J Agric Food Chem*. 2020;68(51):15115-15122. https://doi.org/10.1021/acs.jafc.0c04106.
2 Liu Y, Wang W, Miao J. New antiproliferative dibenzo-*α*-pyrone from whole plants of *Centella asiatica*. *Nat Prod Commun*. 2021;16(3):1-4. https://doi.org/10.1177/1934578X211003019.
3 Amin M, Liang X, Ma X, et al. New pyrone and cyclopentenone derivatives from marine-derived fungus *Aspergillus sydowii* SCSIO 00305. *Nat Prod Res*. 2021;35(2):318-326. https://doi.org/10.1080/14786419.2019.1629919.
4 Xian PJ, Chen HY, Feng Z, et al. Capsulactone: a new 4-hydroxy-*α*-pyrone derivative from an endophytic fungus *Penicillium capsulatum* and its antimicrobial activity. *J Asian Nat Prod Res*. 2021;23(11):1100-1106. https://doi.org/10.1080/10286020.2020.1847092.
5 Hou XF, Song YJ, Zhang M, et al. Enzymology of anthraquinone-*γ*-pyrone ring formation in complex aromatic polyketide biosynthesis. *Angew Chem Int Ed*. 2018;57(41):13475-13479. https://doi.org/10.1002/anie.201806729.
6 Qiu P, Liu JQ, Zhao LS, et al. Inoscavin A, a pyrone compound isolated from a *Sanghuangporus vaninii* extract, inhibits colon cancer cell growth and induces cell apoptosis *via* the hedgehog signaling pathway. *Phytomedicine*. 2022;96:153852. https://doi.org/10.1016/j.phymed.2021.153852.
7 Zhou W, Zhuang YB, Bai YF, et al. Biosynthesis of phlorisovalerophenone and 4-hydroxy-6-isobutyl-2-pyrone in *Escherichia coli* from glucose. *Microb Cell Fact*. 2016;15(1):149. https://doi.org/10.1186/s12934-016-0549-9.
8 Wang MH, Yang LH, Feng LB, et al. Verruculosins A–B, new oligophenalenone dimers from the soft coral-derived fungus *Talaromyces verruculosus*. *Mar Drugs*. 2019;17(9):516. https://doi.org/10.3390/md17090516.
9 Chaiyosang B, Kanokmedhakul K, Sanmanoch W, et al. Bioactive oxaphenalenone dimers from the fungus *Talaromyces macrosporus* KKU-1NK8. *Fitoterapia*. 2019;134:429-434. https://doi.org/10.1016/j.fitote.2019.03.015.
10 Yurchenko EA, Menchinskaya ES, Pislyagin EA, et al. Cytoprotective activity of *p*-terphenyl polyketides and flavuside B from marine-derived fungi against oxidative stress in neuro-2a cells. *Molecules*. 2021;26(12):3618. https://doi.org/10.3390/molecules26123618.
11 Song Q, Yang SQ, Li XM, et al. Aromatic polyketides from the deep-sea cold-seep mussel associated endozoic fungus *Talaromyces minioluteus* CS-138. *Mar Drugs*. 2022;20(8):529. https://doi.org/10.3390/md20080529.
12 Cao X, Ge YC, Lan DH, et al. Spirocyclic polyketides from the marine fungus *Talaromyces* sp. CX11. *Fitoterapia*. 2023;164:105359. https://doi.org/10.1016/j.fitote.2022.105359.
13 Cao X, Shi YT, Wu XD, et al. Talaromylides A–D and talaromytin: polycyclic meroterpenoids from the fungus *Talaromyces* sp. CX11. *Org Lett*. 2019;21(16):6539-6542. https://doi.org/10.1021/acs.orglett.9b02466.
14 Huang ZH, Liang X, Li CJ, et al. Talaromynoids A–I, highly oxygenated meroterpenoids from the marine-derived fungus *Talaromyces purpureogenus* SCSIO 41517 and their lipid accumulation inhibitory activities. *J Nat Prod*. 2021;84(10):2727-2737. https://doi.org/10.1021/acs.jnatprod.1c00681.
15 Li XY, Awakawa T, Mori T, et al. Heterodimeric non-heme iron enzymes in fungal meroterpenoid biosynthesis. *J Am Chem Soc*. 2021;143(50):21425-21432. https://doi.org/10.1021/jacs.1c11548.
16 Zhang M, Yan S, Liang Y, et al. Talaronoids A–D: four fusicoccane diterpenoids with an unprecedented tricyclic 5/8/6 ring system from the fungus *Talaromyces stipitatus*. *Org Chem Front*. 2020;7(21):3486-3492. https://doi.org/10.1039/D0QO00960A.
17 Li Q, Zheng MJ, Li FL, et al. Talarolactones A–G, *α*-pyrone dimers with anti-inflammatory activities from *Talaromyces adpressus*, and their biosynthetic pathways. *Org Lett*. 2023;25(10):1616-1621. https://doi.org/10.1021/acs.orglett.2c04352.
18 Zhang M, Li Q, Li SJ, et al. An unprecedented ergostane with a 6/6/5 tricyclic 13(14→8)*abeo*-8,14-*seco* skeleton from *Talaromyces adpressus*. *Bioorg Chem*. 2022;127:105943. https://doi.org/10.1016/j.bioorg.2022.105943.
19 Zhang M, Deng YF, Liu F, et al. Five undescribed steroids from *Talaromyces stipitatus* and their cytotoxic activities against hepatoma cell lines. *Phytochemistry*. 2021;189:112816. https://doi.org/10.1016/j.phytochem.2021.112816.
20 Chadni Z, Rahaman MH, Jerin I, et al. Extraction and optimisation of red pigment production as secondary metabolites from *Talaromyces verruculosus* and its potential use in textile industries. *Mycology*. 2017;8(1):48-57. https://doi.org/10.1080/21501203.2017.1302013.
21 Morales-Oyervides L, Ruiz-Sanchez JP, Oliveira JC, et al. Biotechnological approaches for the production of natural colorants by *Talaromyces/Penicillium*: a review. *Biotechnol Adv*. 2020;43:107601. https://doi.org/10.1016/j.biotechadv.2020.107601.
22 Jain L, Kurmi AK, Agrawal D. Conclusive selection of optimal parameters for cellulase production by *Talaromyces verruculosus* IIPC 324 under SSF *via* saccharification of acid-pretreated sugarcane bagasse. *Biofuels*. 2018;12(1):61-69. https://doi.org/10.1080/17597269.2018.1449063.
23 Lambre C, Baviera JMB, Bolognesi C, et al. Safety evaluation of the food enzyme containing endo-polygalacturonase and cellulase from the non-genetically modified *Talaromyces cellulolyticus* strain NITE BP-03478. *EFSA J*. 2023;21(2):7840. https://doi.org/10.2903/j.efsa.2023.7840.
24 Hong X, Guan XQ, Lai QL, et al. Characterization of a bioactive meroterpenoid isolated from the marine-derived fungus *Talaromyces* sp. *Appl Microbiol Biotechnol*. 2022;106(8):2927-2935. https://doi.org/10.1007/s00253-022-11914-1.
25 Zang Y, Genta-Jouve G, Escargueil AE, et al. Antimicrobial oligophenalenone dimers from the soil fungus *Talaromyces stipitatus*. *J Nat Prod*. 2016;79(12):2991-2996. https://doi.org/10.1021/acs.jnatprod.6b00458.
26 Zang Y, Genta-Jouve G, Retailleau P, et al. Talaroketals A and B, unusual bis (oxaphenalenone) spiro and fused ketals from the soil fungus *Talaromyces stipitatus* ATCC 10500. *Org Biomol Chem*. 2016;14(9):2691-2697. https://doi.org/10.1039/C5OB02657A.
27 Cong MJ, Zhang Y, Feng XY, et al. Anti-inflammatory alkaloids from the cold-seep-derived fungus *Talaromyces helicus* SCSIO41311. *3 Biotech*. 2022;12(8):161. https://doi.org/10.1007/s13205-022-03237-9.
28 Asai T, Chung YM, Sakurai H, et al. Tenuipyrone, a novel skeletal polyketide from the entomopathogenic fungus, *Isaria tenuipes*, cultivated in the presence of epigenetic modifiers. *Org Lett*. 2012;14(2):513-515. https://doi.org/10.1021/ol203097b.
29 Luo JG, Wang XB, Xu YM, et al. Delitschiapyrone A, a pyrone-naphthalenone adduct bearing a new pentacyclic ring system from the leaf-associated fungus *Delitschia* sp. FL1581. *Org Lett*. 2014;16(22):5944-5947. https://doi.org/10.1021/ol502973c.
30 Li FL, Ye Z, Huang ZY, et al. New *α*-pyrone derivatives with herbicidal activity from the endophytic fungus *Alternaria brassicicola*. *Bioorg Chem*. 2021;117:105452. https://doi.org/10.1016/j.bioorg.2021.105452.
31 Ohtani I, Kusumi T, Kashman Y, et al. High-field FT NMR application of Mosher's method. The absolute configurations of marine terpenoids. *J Am Chem Soc*. 1991;113(11):4092-4096. https://doi.org/10.1021/ja00011a006.
32 Zheng MJ, Zhou CX, Liao H, et al. Enantiomeric *α*-pyrone derivatives with immunosuppressive activity from *Talaromyces adpressus*. *Phytochemistry*. 2023;218:113931. https://doi.org/10.1016/j.phytochem.2023.113931.
33 Zheng MJ, Xiao Y, Li Q, et al. Cytotoxic ergosteroids from a strain of the fungus *Talaromyces adpressus*. *J Nat Prod*. 2023;86(9):2081-2090. https://doi.org/10.1021/acs.jnatprod.3c00089.